Journal of Power Sources 196 (2011) 10183–10190

Contents lists available at ScienceDirect

Journal of Power Sources

journal homepage: www.elsevier.com/locate/jpowsour

Investigation of compatible anode systems for $LaNbO_4$-based electrolyte in novel proton conducting solid oxide fuel cells

Anna Magrasó[a,*], Marie-Laure Fontaine[b]

[a] Department of Chemistry, Centre for Materials Science and Nanotechnology, University of Oslo, FERMiO, Forskningsparken, Gaustadalleen 21, NO-0349 Oslo, Norway
[b] SINTEF Materials and Chemistry, NO-0314 Oslo, Norway

ARTICLE INFO

Article history:
Received 21 April 2011
Received in revised form 13 July 2011
Accepted 16 July 2011
Available online 17 August 2011

Keywords:
Anode
PC-SOFC
Chemical compatibility
$LaNbO_4$
La_3NbO_7
$LaNb_3O_9$

ABSTRACT

In the current manufacturing process of novel $LaNbO_4$-based proton conducting fuel cells a thin layer of the electrolyte is deposited by wet ceramic coating on NiO–$LaNbO_4$ based anode and co-sintered at 1200–1300 °C. The chemical compatibility of NiO with acceptor doped $LaNbO_4$ material is crucial to ensure viability of the cell, so potential effects of other phases resulting from off-stoichiometry in acceptor doped $LaNbO_4$ should also be explored. Compatibility of NiO with Ca-doped $LaNbO_4$ and its typical off-set compositions (La_3NbO_7 and $LaNb_3O_9$) are investigated in this work. It is shown that while NiO does not react with Ca-doped $LaNbO_4$, fast reaction occurs with La_3NbO_7 or $LaNb_3O_9$. La_3NbO_7 and NiO form a mixed conducting perovskite phase $LaNi_{2/3}Nb_{1/3}O_3$, while $LaNb_3O_9$ and NiO form either $NiNb_2O_6$ or $Ni_4Nb_2O_9$ depending on the annealing temperature. This implies that manufacturing $LaNbO_4$-based proton conducting fuel cells requires a strict control of the stoichiometry of the electrolyte.

1. Introduction

During the past years, novel proton conducting solid oxide fuel cells (PC-SOFCs) integrating alkaline doped $LnNbO_4$ electrolytes have been thoroughly investigated as potential candidates for overcoming current challenges of this technology. The recently discovered acceptor-doped rare earth ortho-niobate oxides show good chemical stability in steam and carbon containing atmospheres, sufficient mechanical strength and have reasonably low sintering temperature compared to other ceramic proton conducting materials. Acceptor-doped lanthanum ortho-niobate ($LaNbO_4$) exhibits proton conductivities close to 0.001 S cm^{-1} for $La_{0.99}Ca_{0.01}NbO_4$ under 2.5% H_2O at ~950 °C [1,2]. These materials are thus of potential use as electrolytes for PC-SOFCs, provided that thin layers of ~1 to 2 μm thick are manufactured to achieve acceptable electrolyte resistances. For the production of single cells, highly performing and compatible electrodes have to be developed. Nickel is often chosen as the main anode component because it exhibits the highest electrochemical activity towards oxidation of H_2. As manufacturing of the cell is often carried out in air, NiO is commonly used during cell assembly, and Ni is obtained during *in situ* reduction of the complete cell. While it is obvious that acceptor doped $LaNbO_4$ should not react with Ni during cell operation, it is also essential that NiO does not react during fabrication with $LaNbO_4$, its Ca-doped analogue, and $LaNbO_4$ off-stoichiometric compositions. We will demonstrate in this work that the presence of these phases have an important impact on the microstructure at the interface between the electrode–electrolyte and this may lead to detrimental effects on $LaNbO_4$-based fuel cells performance, as already mentioned in Ref. [3].

It has recently been shown that $LaNbO_4$ is a "line" compound and offset from the nominal 1:1 ratio between La and Nb cations leads to the formation of La_3NbO_7 or $LaNb_3O_9$ as secondary phases [4]. Additionally, the use of an alkali earth dopant (typically Sr or Ca), which is necessary to improve the protonic conductivity, can also contribute to the formation of additional secondary phases. The solubility limit of alkali earth cations in $LaNbO_4$ is very low, in the range of 0.5 to 1 mol.% but has not yet been precisely determined. The large number of binary and ternary oxide compounds reported in the phase diagrams AO–La_2O_3–Nb_2O_5 (A = Ca, Sr) [5,6] gives rise to significant challenges for controlling material's stoichiometry. Thorough investigation of acceptor doped $LaNbO_4$ materials prepared by spray-pyrolysis points out that traces of La_3NbO_7 or $LaNb_3O_9$ are always present, though their extent varies depending on the synthesis procedures [7]. It is therefore important to determine not only whether NiO reacts with $LaNbO_4$, but also with these additional, unintentional phases.

This work reports on the compatibility between NiO and niobate phases in screen-printed $La_{0.995}Ca_{0.005}NbO_4$ (LCNO):NiO composite anodes deposited on self-supported LCNO electrolyte. Various

* Corresponding author. Tel.: +47 22840660; fax: +47 22840651.
E-mail addresses: annamagraso@gmail.com, a.m.sola@smn.uio.no (A. Magrasó).

0378-7753/$ – see front matter © 2011 Elsevier B.V. All rights reserved.
doi:10.1016/j.jpowsour.2011.07.089

annealing temperatures are applied to investigate effects of secondary phases on the composition and the microstructure of the anode and the interface anode/electrolyte. Reaction sintering between NiO and single phase La_3NbO_7 or $LaNb_3O_9$ materials is also carried out to support this investigation and to identify the reaction products.

2. Experimental work

2.1. Materials synthesis

NiO powder was purchased at GFS Chemical. Two batches of LCNO material were produced by spray-pyrolysis at the Norwegian University of Science and Technology (NTNU) as sub-micron particle size powders as described in Ref. [5] and references therein. The first batch contained single phase $La_{0.995}Ca_{0.005}NbO_4$ powder (batch I), while the second batch additionally contained traces of secondary niobate phases (batch II). The amount of secondary phase was not known, but was estimated to be below 2–3%, since laboratory X-ray diffraction patterns showed the reflections of $LaNbO_4$ only. Both single phase La_3NbO_7 and $LaNb_3O_9$ were prepared by solid state reaction according to a procedure already described [8,9], and $La(Ni_{2/3}Nb_{1/3})O_3$ was synthesized by a polymeric route as reported in Ref. [10].

2.2. Reaction sintering between NiO and lanthanum niobate oxides

Powder mixtures containing 50 wt.% of NiO and 50 wt.% of La_3NbO_7 or $LaNb_3O_9$ were ball milled in isopropanol for 1 h at 250 rpm. NiO is in excess (molar-wise). The mixtures were dried, pressed into pellets, and annealed in air at 1200, 1300, 1400 and 1500 °C for 5 h with both heating and cooling rates of 200 °C h^{-1}.

2.3. Screen-printing of NiO–LCNO composite anodes on a dense LCNO electrolyte support

Inks of NiO:LCNO (40 vol.% Ni) were prepared by mixing NiO powder and LCNO powder from batch II with a commercial organic binder vehicle (Heraeus V006) and terpineol. The mixing was carried out in a planetary miller at 300 rpm for several hours. The inks were screen-printed on dense self-supported LCNO electrolyte pellets (made out of LCNO batch II), which were sintered in air at 1400 °C for 5 h. For comparison, additional electrolyte supports were produced using LCNO powder from batch I to coat a NiO layer anode. Prior to the deposition of the anodes, the pellets were polished using SiC grinding paper and then washed in ethanol. The as-deposited composite layers were dried in air at 90 °C, and further annealed at 1150–1400 °C for 2 h, in air.

2.4. Characterization of materials

Samples were examined by a field emission gun scanning electron microscope (SEM; FEG Quanta 200 FEI) equipped with X-ray energy dispersive spectroscopy (EDS; EDAX) and by X-ray diffraction (XRD; SIEMENS D5000). Thermogravimetric analysis (TGA; SDT 2960 from TA Instruments) of $La(Ni_{2/3}Nb_{1/3})O_3$ in powder form was carried out in 5% dry H_2 balanced with Ar upon annealing from room temperature up to 550 °C or 1200 °C with both heating and cooling rates of 10 °C min^{-1}.

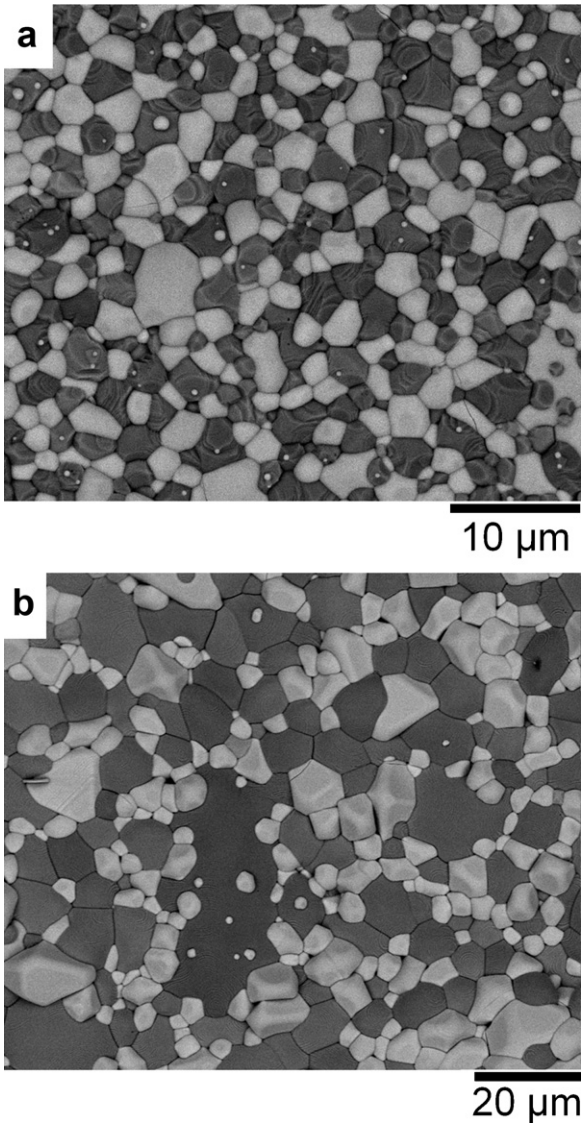

Fig. 1. Representative SEM micrographs of a 40 vol. % NiO–LCNO composite annealed at (a) 1200 and (b) 1400 °C, from Ref. [11].

3. Results

3.1. Reactivity between NiO and LCNO from batch I

XRD and SEM analyses carried out on solid state sintered NiO and LCNO powder from batch I did not reveal formation of secondary phases, as reported in Ref. [11], even after annealing in air at 1400 °C. Representative micrographs are shown in Fig. 1. Transmission electron microscopy and X-ray photoelectron spectroscopy also confirm that no interdiffusion or formation of any secondary phases occur at the interface between NiO and acceptor doped $LaNbO_4$ [12,13]. These results are consistent with the NiO–La_2O_3–Nb_2O_5 ternary phase diagram, which does not predict any reaction between NiO and $LaNbO_4$ [14].

3.2. Reactivity between NiO and La_3NbO_7 as a function of temperature

The diffraction patterns obtained after annealing a mixture of La_3NbO_7 and NiO at various temperatures are displayed in Fig. 2. The reaction results in a new phase with the perovskite-type structure, which forms at 1200 °C along with a minor amount of La_3NbO_7

Table 1
Summary of the lattice parameters of NiO and La_3NbO_7, and the reaction products before and after each thermal treatment (TT) obtained by the Le Bail refinement method.

		Literature values	Before TT	1200 °C	1300 °C	1400 °C	1500 °C
NiO *Fm*−3*m* (pdf: 04-0835)	*a* (Å)	4.177	4.176	4.176	4.177	4.177	4.178
La_3NbO_7 *Cmcm* (pdf: 71-1345)	*a* (Å) *b* (Å) *c* (Å)	11.167 7.629 7.753	11.155 7.634 7.755	<3% (not refined)	Not detected	Not detected	Not detected
$La(Ni_{2/3}Nb_{1/3})O_3$ *P*2/*n* (Ref. [10])	*a* (Å) *b* (Å) *c* (Å)	5.582 5.619 7.905	–	5.588 5.633 7.917	5.586 5.636 7.915	5.584 5.638 7.914	5.586 5.640 7.917

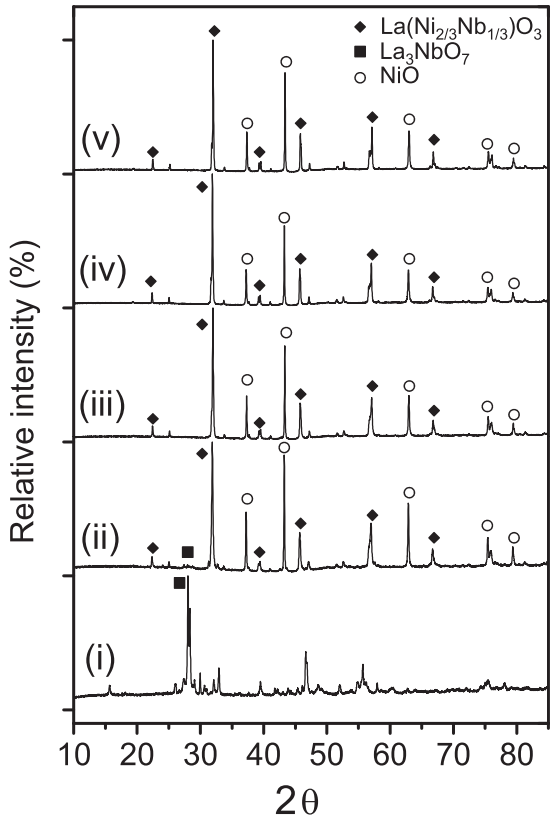

Fig. 2. XRD patterns for the reaction products between La_3NbO_7 (i) and NiO after annealing at 1200 (ii), 1300 (iii), 1400 (iv) and 1500 °C (v).

(and NiO – excess). The reaction is complete at 1300 °C, and the XRD pattern of the annealed mixture does not change significantly between 1300 °C and 1500 °C. The new phase corresponds to $La(Ni_{2/3}Nb_{1/3})O_3$, recently reported by Tolchard et al. [10]. The lattice parameters obtained by the Le Bail refinement method [15] for the reactants and the products fall within the values reported in the literature for the identified oxides (Table 1).

The observation of the reaction products by SEM (Fig. 3) is consistent with the XRD results; EDS only detects two phases containing Ni and O (dark phase in the micrograph) corresponding to NiO, and another phase containing La, Ni, Nb and O (white phase). It can also be seen that the new phase has sustained grain growth during annealing from 1200 °C to 1500 °C. From these results, it is found that the following chemical reaction can be expected at temperatures equal and above 1200 °C:

$$1/3La_3NbO_7 + 2/3NiO \rightarrow La(Ni_{2/3}Nb_{1/3})O_3 \quad (1)$$

Additional TGA reveals that the perovskite is not stable under reducing conditions, as shown by the thermal decomposition and post-analysis of $La(Ni_{2/3}Nb_{1/3})O_3$ powder in dried 5% H_2 upon annealing up to 1200 °C (see Fig. 4). There is a small weight loss below 550 °C that probably corresponds to evaporation of water and/or decomposition of remaining organics. XRD at point 1 shows essentially no differences compared to the as-synthesized powder. The second step starts above 800 °C, is completed at 1100 °C and is characterized by a weight loss of ~4.4%. This probably corresponds to the full reduction of Ni^{2+} to Ni (the theoretical is 4.15%). An evidence of the decomposition is shown by the presence of metallic Ni and La_3NbO_7 (XRD at point 2, c.f. Fig. 4). Subsequent annealing in air of the latter at 800 °C yields to the formation of NiO nanoparticles and La_3NbO_7.

3.3. Reactivity between NiO and $LaNb_3O_9$ as a function of temperature

The diffraction patterns of the reaction products after annealing $LaNb_3O_9$ and NiO at various temperatures are depicted in Fig. 5. It can be seen that $LaNb_3O_9$ reacts with NiO to form $NiNb_2O_6$ and $LaNbO_4$ at 1200 °C, in accordance with XRD combined with SEM/EDS analyses. The observation by SEM (Fig. 6a) shows the presence of several phases with different morphologies. The phase

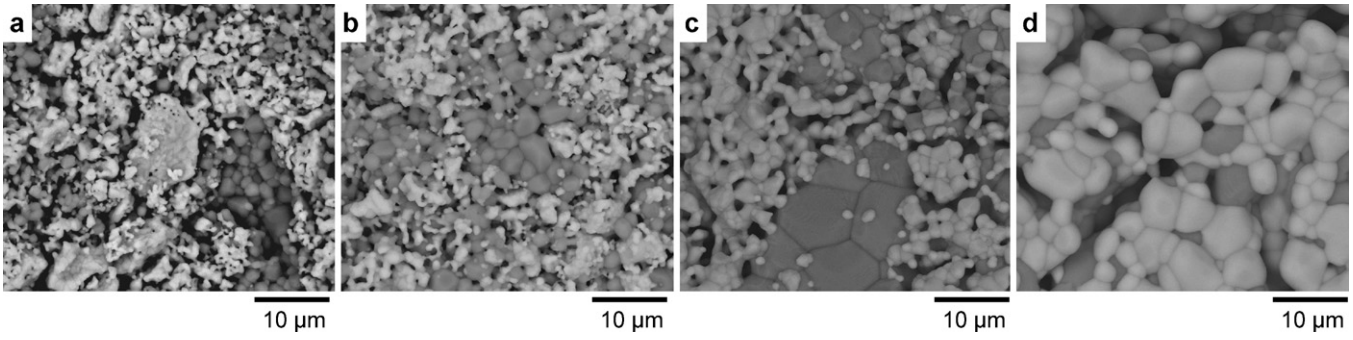

Fig. 3. SEM micrographs of the reaction products between La_3NbO_7 and NiO after annealing at (a) 1200, (b) 1300, (c) 1400, and (d) 1500 °C.

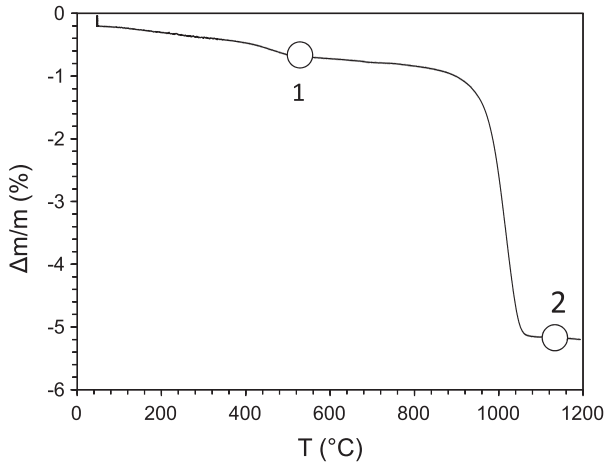

Fig. 4. Thermal decomposition of $La(Ni_{2/3}Nb_{1/3})O_3$ powder from RT to 1200 °C in dry 5% H_2/Ar. XRD patterns were collected at the points marked as 1 and 2.

with spherical-like grains corresponds to NiO, while the phase with acicular-shaped grains contains mostly Ni and Nb. The Ni:Nb ratio of this composition is about 0.5–0.7 by EDS analysis.

Higher annealing temperature results in the formation of $Ni_4Nb_2O_9$. NiO is still present at all temperatures (it is in excess). The lattice parameters of $NiNb_2O_6$ and $Ni_4Nb_2O_9$ obtained from XRD after each thermal treatment are listed in Table 2. SEM micrographs of the reaction products after annealing at 1300–1400 °C (Fig. 6b and c) show the presence of at least three phases of different morphology and composition: the darker phase corresponds to NiO, the white phase to $LaNbO_4$, and the grey grains contain both Ni and Nb. The Ni:Nb ratio is about 2–2.5 from EDS. Hence, these results are in accordance with the formation of $Ni_4Nb_2O_9$.

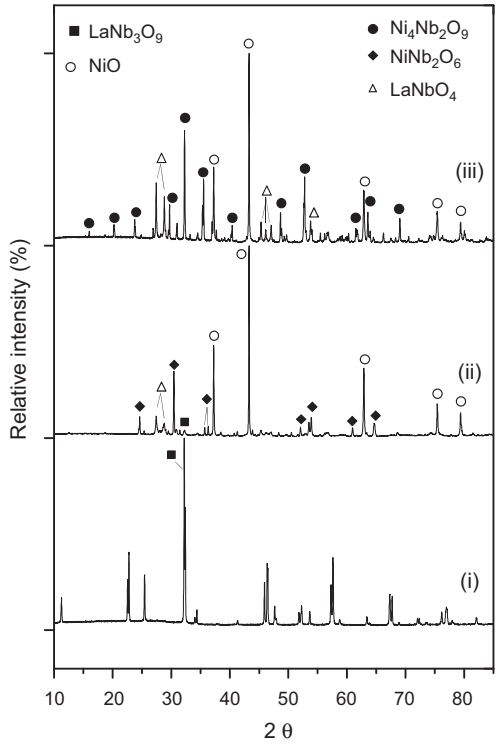

Fig. 5. XRD patterns for the reaction products between $LaNb_3O_9$ (i) and NiO after annealing at 1200 (ii), and 1300 °C (iii).

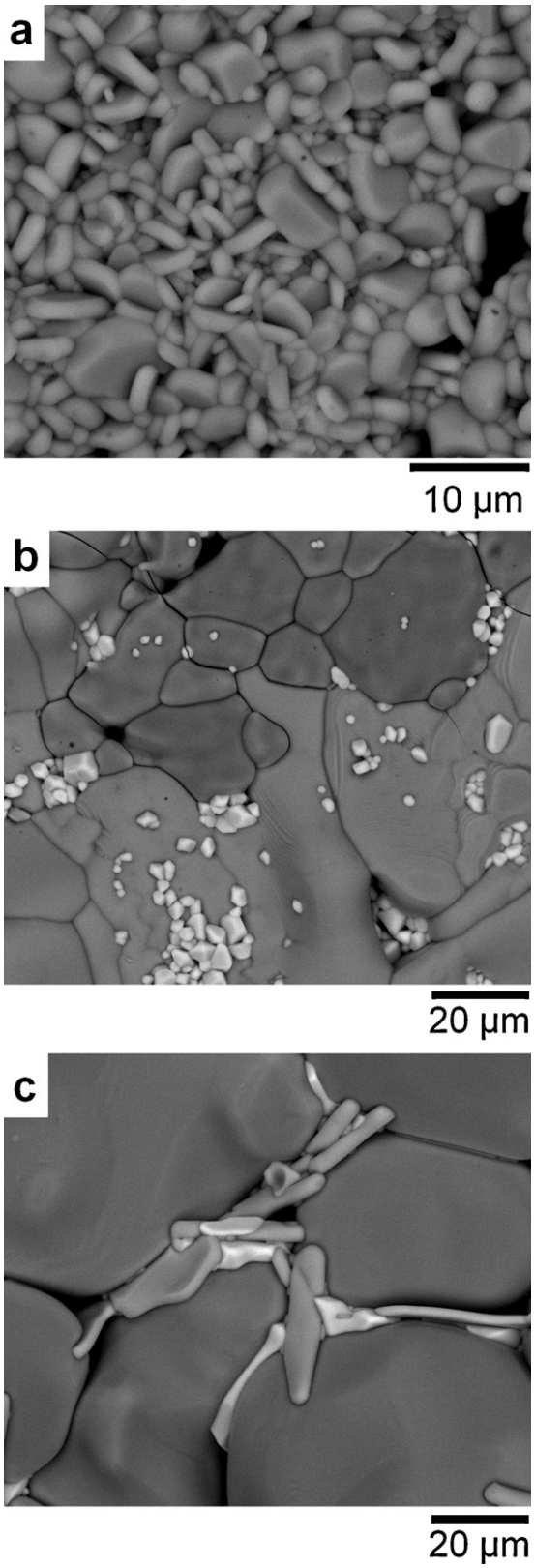

Fig. 6. SEM micrographs of the reaction products between $LaNb_3O_9$ and NiO after annealing at (a) 1200, (b) 1300, and (c) 1400 °C.

Table 2
Summary of the lattice parameters of NiO and $LaNb_3O_9$, and the reaction products before and after each thermal treatment (TT) obtained by the Le Bail refinement method.

		Literature values	Before TT	1200 °C	1300 °C	1400 °C
NiO *Fm*−3*m* (pdf:04-0835)	*a* (Å)	4.177	4.177	4.176	4.176	4.176
$LaNb_3O_9$ *P*4/*mmm* (pdf: 32-0496)	*a* (Å) *c* (Å)	3.911 7.908	3.917 7.915	Not detected	Not detected	Not detected
$LaNbO_4$ *I*2/*a* (pdf: 32-0496)	*a* (Å) *b* (Å) *c* (Å) *β* (°)	5.204 11.521 5.568 94.09	5.203 11.523 5.564 94.04	5.216 11.524 5.553 93.74	5.205 11.520 5.565 93.95	5.204 11.525 5.567 94.03
$NiNb_2O_6$ *Pbcn* (pdf: 31-0906)	*a* (Å) *b* (Å) *c* (Å)	14.022 5.675 5.015	–	14.036 5.676 5.020	Not detected	Not detected
$Ni_4Nb_2O_9$ *Pcan* (pdf:77-2409)	*a* (Å) *b* (Å) *c* (Å)	5.055 8.769 14.304	–	<3% (not refined)	5.026 8.760 14.335	5.031 8.760 14.354

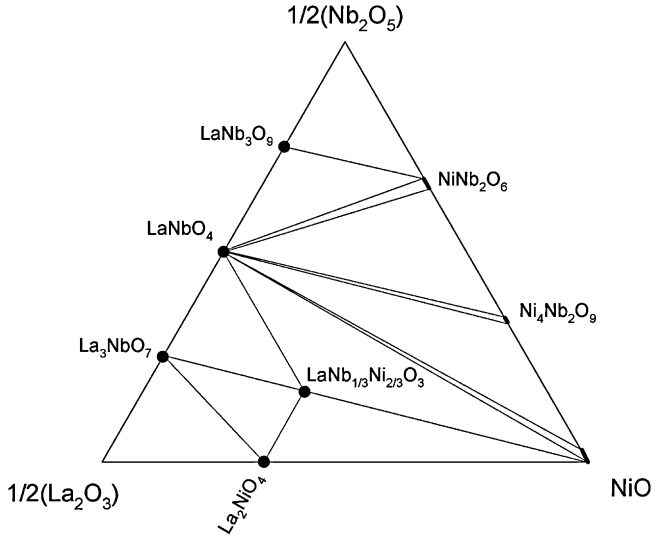

Fig. 7. La_2O_3–Nb_2O_5–NiO ternary phase diagram at 1250 °C, modified from Tolchard et al. [10].

One may, therefore write the following reactions:

$$LaNb_3O_9 + NiO \rightarrow NiNb_2O_6 + LaNbO_4 \quad (\sim 1200\,^{\circ}C) \tag{2}$$

$$NiNb_2O_6 + 3NiO \rightarrow Ni_4Nb_2O_9 \quad (\geq 1300\,^{\circ}C) \tag{3}$$

This implies that $LaNb_3O_9$ will react with NiO at temperatures equal and above 1200 °C, which is a minimum temperature needed to obtain well adhered electrode composites on the LCNO electrolyte. The phases formed during high temperature annealing will depend on temperature. These findings are in accordance with the phase diagram of NiO–La_2O_3–Nb_2O_5 [14,16], as $NiNb_2O_6$ is a stable ternary compound being almost stoichiometric after sintering at 1200 °C [17]. $Ni_4Nb_2O_9$ is not stable at 1200 °C [17], and starts to form from $NiNb_2O_6$ and NiO only at relatively high temperatures (~1250 °C and above) [16,18]. The phase diagram with the relevant phases at 1250 °C is drawn in Fig. 7 after Tolchard et al. [10].

3.4. Investigation of NiO–LCNO screen-printed anodes

Screen-printed NiO–LCNO composite anodes deposited on dense LCNO electrolyte from batch II were annealed in air at temperatures ranging from 1150 °C to 1400 °C. All samples present on their surface a relatively well defined "segregation rim", which extends over more than ~100 μm (at 1200 °C) from the composite anode and outwards over the dense electrolyte surface. In some samples, it was also possible to observe these secondary phases in cross-section view at the interface between the Ni–LCNO anode and LCNO electrolyte. The centre of the anode, on the other hand, does not exhibit secondary phases, and only NiO and $LaNbO_4$ can be seen.

The surface of NiO–LCNO anode annealed at 1200 °C is shown in Fig. 8. One can clearly observe the formation of a secondary phase with acicular-like shape along the rim (c.f. inset in Fig. 8a), while the surface at the centre of the composite looks unreacted (Fig. 8c) and similar to that shown in Fig. 1. EDS analyses of the segregation rim detected a Nb:Ni:La composition of about $1:(0.6 \pm 0.2):(0.2 \pm 0.2)$. The corresponding spectrum is shown in Fig. 9(iv), and is relatively similar to the one obtained for the $NiNb_2O_6$ phase described in Section 3.3.

The microstructure at the rim does not change dramatically from 1200 to 1250 °C (Fig. 10a and b), though the size and extent of formation of secondary phases increase. At temperatures higher than 1300 °C, the microstructure at the rim evolves into a new phase with melted appearance (Fig. 10c and d). The extent of segregation has increased further at these high temperatures, and the segregation rim is no longer confined to the interface electrode–electrolyte, but also diffuses into the anode composite. EDS analysis detected a Nb:Ni:La composition of about $1:(2.5 \pm 0.3):(0.1 \pm 0.1)$. The corresponding spectrum is shown in Fig. 9(v) and shows similarities to the one presented in Section 3.3 for $Ni_4Nb_2O_9$.

In order to confirm the identified phases, X-ray patterns of the surface of the specimens were recorded and are shown in Fig. 11. It is found that the samples annealed between 1150 °C and 1250 °C contain $NiNb_2O_6$ (pdf: 72-0481), in accordance with microanalysis given by EDS and the typical morphology of this phase. At temperatures above 1300 °C, the peaks may be identified as $Ni_4Nb_2O_9$ (pdf: 77-2409). We should mention that the available structural model of $Ni_4Nb_2O_9$ does not fully fit all reflections corresponding to the new phase, as intensity and position of some of the peaks are slightly shifted. For this reason, a new structural model for this phase is under investigation by transmission electron microscopy [19].

In order to explain the formation of these secondary phases, a closer inspection of the electrolyte before screen-printing NiO–LCNO composite was carried out (Fig. 12). XRD analysis only reveals the presence of LCNO phase, and its typical microstructure is shown in Fig. 12a. However, careful SEM observations show that some regions at the surface of LCNO pellets have other compositions (Fig. 12b and c). A Nb-rich phase is detected as a darker phase under the back-scattered detector, or as small cube-shaped

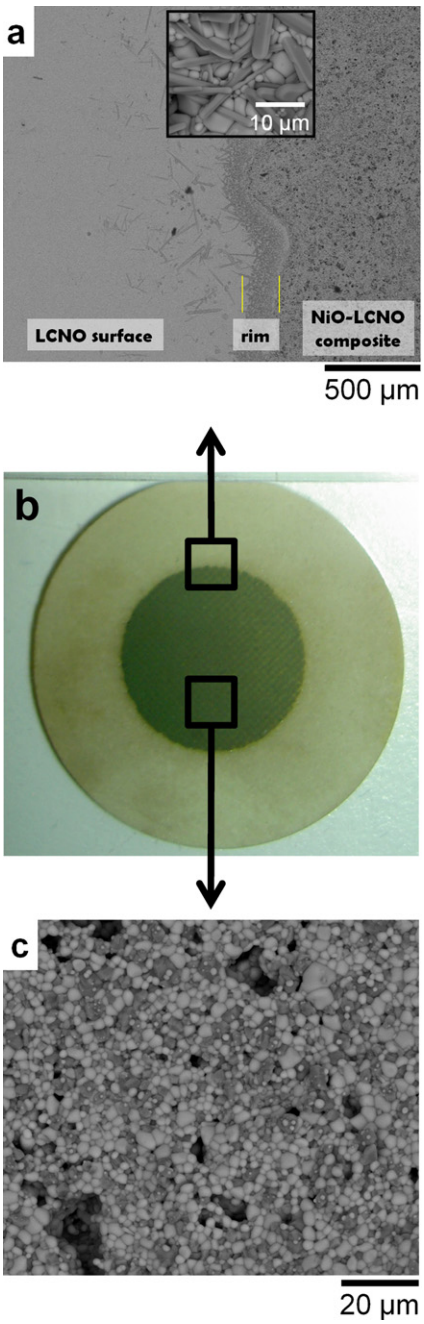

Fig. 8. (a) SEM micrographs of a low magnification view of the rim electrode–electrolyte; inset shows the microstructure of the segregated phase at the rim, (b) photograph of a screen printed NiO–LCNO composite on a LCNO electrolyte support annealed at 1250 °C, and (c) a SEM micrograph of the NiO–LCNO composite.

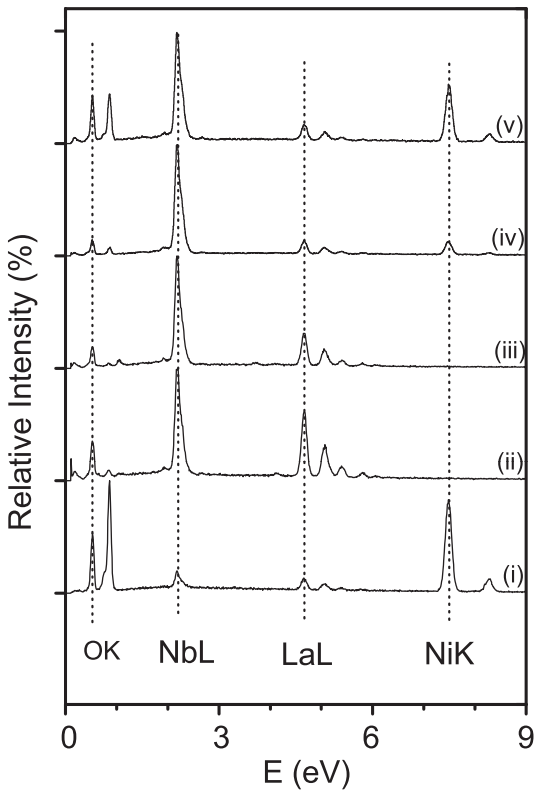

Fig. 9. Representative EDS spectrums of (i) a NiO particle in a NiO-$LaNbO_4$ composite, (ii) $LaNbO_4$ (electrolyte) (iii) $LaNb_3O_9$ (in the electrolyte), (iv) $NiNb_2O_6$ (at the rim) and (v) $Ni_4Nb_2O_9$ (at the rim/electrode). All lines can be identified as O, Ni, Nb or Ni, but only the main lines for each element are highlighted, for simplicity.

crystals. Analysis by EDS of these phases reveal a La:Nb ratio of around 1:3 (c.f. Fig. 9(iii)), and can be ascribed to $LaNb_3O_9$. $LaNbO_4$ and $LaNb_3O_9$ can form a liquid phase around ~1370 °C according to the La_2O_3–Nb_2O_5 phase diagram, and this could explain the melted appearance in the micrograph at Fig. 12b, since the electrolyte was sintered at 1400 °C. We can therefore conclude that $LaNb_3O_9$ at the surface of a LCNO pellet has reacted with NiO at high temperatures at the electrode–electrolyte rim to form $NiNb_2O_6$ or $Ni_4Nb_2O_9$, and it is the presence of this phase that is the responsible of the appearance of the "segregation rim".

LCNO dense pellet made from batch I powder, which does not contain La_3NbO_7 or $LaNb_3O_9$, was used to screen-print ink of pure NiO. After annealing at 1250 °C, the interface was free of secondary phases through the entire rim (see Fig. 13), which means that obtaining powders with suitable LCNO stoichiometry is possible and otherwise essential in order to control the reactivity at the NiO–LCNO interface.

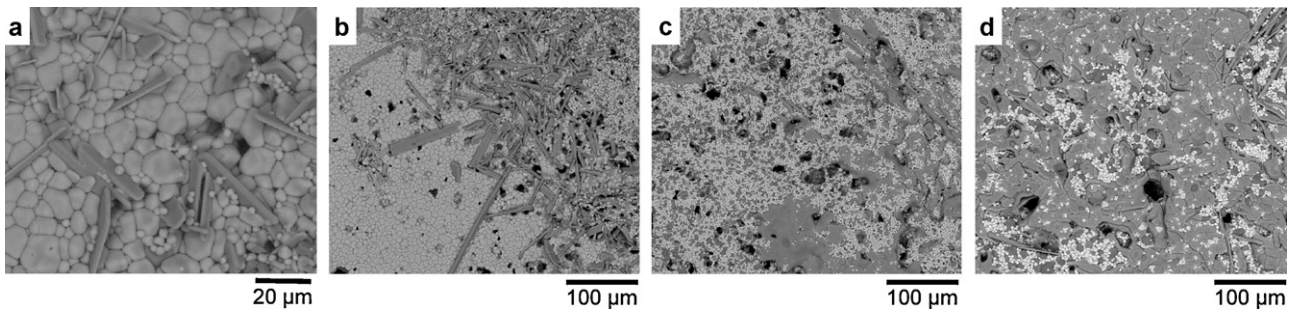

Fig. 10. Microstructural evolution of the rim electrolyte–electrode with temperature after annealing at 1200 (a), 1250 (b), 1300 (c) and 1400 °C (d).

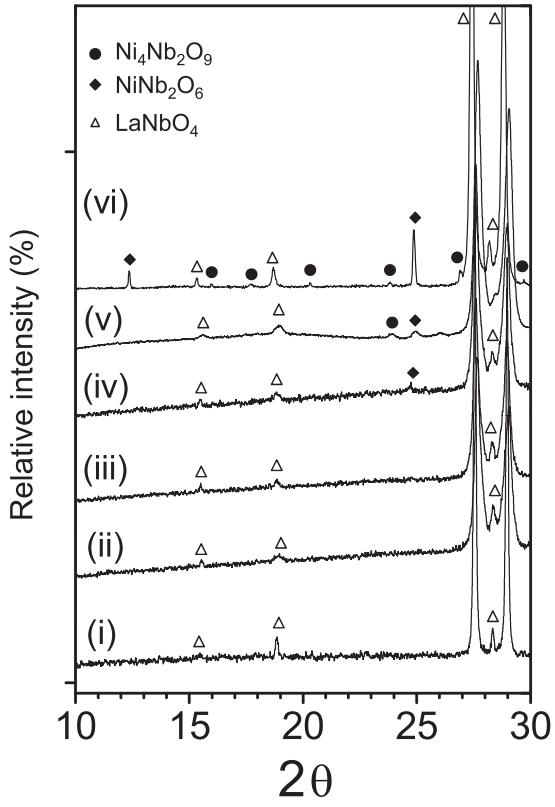

Fig. 11. Selected area of the XRD patterns of Ca:$LaNbO_4$ support before (i) and after coating a screen-printed NiO–Ca:$LaNbO_4$ composite and annealing at 1150 °C (ii), 1200 °C (iii), 1250 °C (iv), 1300 °C (v) and 1400 °C (vi).

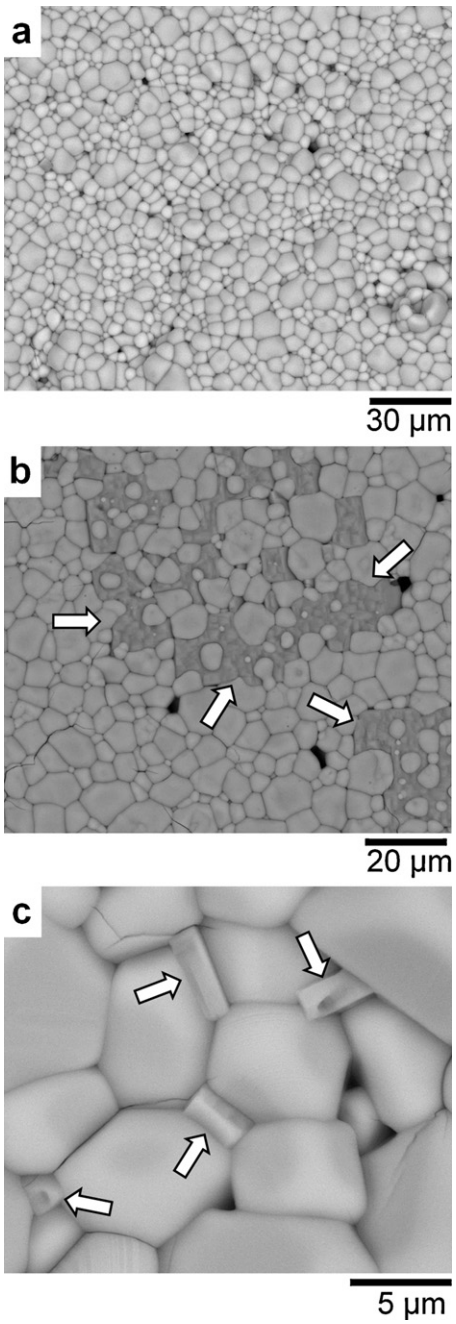

Fig. 12. SEM micrograph of (a) the surface of $LaNbO_4$, and (b and c) selected areas of the same surface showing the presence of Nb-rich phases, which correspond to $LaNb_3O_9$.

4. Discussion

It has been previously demonstrated that there is no chemical reaction between NiO and $LaNbO_4$ (and/or Ca-doped $LaNbO_4$) [11–14], but the presence of off-stoichiometric $LaNbO_4$ containing traces of La_3NbO_7, or $LaNb_3O_9$, promotes the formation of additional secondary phases during the consolidation of the anode. It is presently shown that La_3NbO_7 reacts with NiO to form $La(Ni_{2/3}Nb_{1/3})O_3$, and $LaNb_3O_9$ forms $NiNb_2O_6$ or $Ni_4Nb_2O_9$, depending on the annealing temperature.

It is relevant to foresee possible effects of these secondary phases on the electrochemical behaviour of a single cell. $NiNb_2O_6$ belongs to a family of materials with the columbite structure [20], and the transport properties of columbite-type phases have been determined for a variety of compositions [21–23]. The activation energy for electrical transport in $NiNb_2O_6$ is high (~1.3 eV), and the overall conductivity is low, in the order of 10^{-5} S cm^{-1} at 700 °C in air [22]. $Ni_4Nb_2O_9$ has a corundum-type structure [17], and its conductivity, probably mainly due to electron holes, has been recently reported to be ~10^{-3} to 10^{-4} S cm^{-1} at 700–800 °C in Ar–O_2 mixtures, and to present weak dependence with pO_2 [24]. $La(Ni_{2/3}Nb_{1/3})O_3$ is a new material with a perovskite-type structure, its electrical characterization is under investigation [25]. The total conductivity for this material is ~0.2 S cm^{-1} at 700 °C in wet O_2, and the proton conductivity could not be measured, but it is likely to be below 10^{-5} S cm^{-1} [25]. Therefore, one might expect that the presence of any of these phases will negatively affect the performance of the anode systems due to their low conductivity, both electronic and protonic.

The electrolyte thickness in $LaNbO_4$ based fuel cells must be in the micron range to minimize ohmic losses and reach an acceptable PC-SOFC performance. The compatibility of the electrodes used during the processing of anode supported-cells is therefore critical. If a green electrolyte layer contains $LaNb_3O_9$ or La_3NbO_7, this phase will react with NiO during sintering, which is usually fired above 1200 °C to obtain dense and gas-tight electrolyte and a well adhered interface. Depending on the extent of non-stoichiometry, the interface may be damaged since the reacted phases will form between the electrolyte and the anode. Since all these phases present insufficient electronic conductivity to act as current collectors, and, expectedly, lower proton conductivity than LCNO, this will probably limit current collection and/or block the electrochemical reaction thus deriving into a highly resistive interface. Formation of cracks, pinholes, or other microstructural effects can also be expected to occur, depending on the amount of undesired phases.

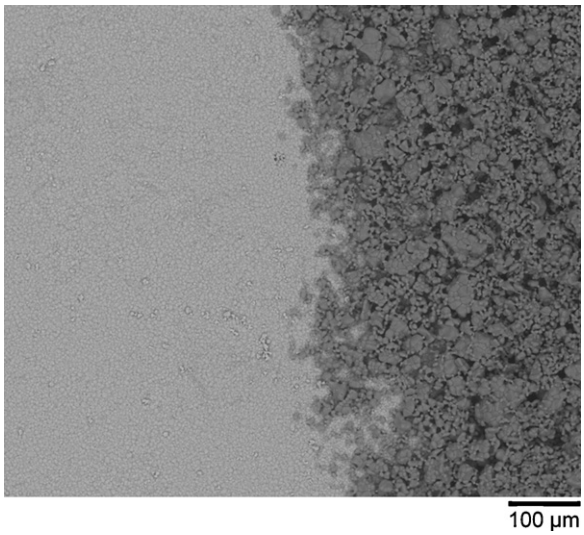

Fig. 13. Representative SEM micrograph of a segregation-free NiO with LCNO rim interface.

Fabrication of fuel cells based on thick [3,26,27] and thin [28] films of $LaNbO_4$ supported on a NiO–$LaNbO_4$ cermet have been reported and are possible to produce, but where careful stoichiometry control of the electrolyte is essential, in particular, for thin-film based fuel cells.

5. Conclusions

$LaNbO_4$ is a "line" compound, and offset from the nominal La:Nb ratio 1:1 leads to the formation of either La_3NbO_7 or $LaNb_3O_9$ secondary phases. We have demonstrated that NiO reacts with both La_3NbO_7 and $LaNb_3O_9$, while $LaNbO_4$ does not. La_3NbO_7 and NiO powder mixtures form $LaNi_{2/3}Nb_{1/3}O_3$, while $LaNb_3O_9$ and NiO form either $NiNb_2O_6$ or $Ni_4Nb_2O_9$, depending on the final annealing temperature. Considering the respective properties of these phases, it is foreseen that their presence will negatively affect the performance of single cells and/or simply create microstructural defects that may be detrimental for its final usage. This means that manufacturing $LaNbO_4$-based proton conducting fuel cells requires a strict control of the stoichiometry of LCNO materials.

Acknowledgements

Authors would like to greatly acknowledge G.E. Syvertsen for lending a critical eye to the manuscript, Dr. Tolchard for his help in building up the phase diagram of this work, and the colleagues at CNRS IEM for their technical contribution to thermogravimetric analysis. Support from the NANOMAT "nanoPCFC" project (182090/510) of the Research Council of Norway is gratefully acknowledged.

References

[1] R. Haugsrud, T. Norby, Nat. Mater. 5 (2006) 193.
[2] R. Haugsrud, T. Norby, Solid State Ionics 177 (2006) 1129–1135.
[3] A. Magrasó, M.-L. Fontaine, Y. Larring, R. Bredesen, G.E. Syvertsen, H.L. Lein, T. Grande, M. Huse, R. Strandbakke, R. Haugsrud, T. Norby, Fuel Cells 11 (1) (2011) 17–25.
[4] G.E. Syvertsen, et al., in preparation.
[5] T. Mokkelbost, I. Kaus, R. Haugsrud, T. Norby, T. Grande, M.-A. Einarsrud, J. Am. Ceram. Soc. 91 (2008) 879–886.
[6] A.M. Frolov, A.A. Evdokimov, Russ. J. Inorg. Chem. (Engl. Transl.) 32 (1987) 1771.
[7] G.E. Syvertsen, A. Magrasó, R. Haugsrud, Mari-Ann Einarsrud, T. Grande, submitted for publication.
[8] R. Haugsrud, T. Risberg, J. Electrochem. Soc. 156 (2009) B425–B428.
[9] Jaran R. Wood, Defects and conductivity in Sr-doped $LaNb_3O_9$, M.Sc. Thesis, University of Oslo, 2007.
[10] J.R. Tolchard, M.-L. Fontaine, T. Grande, Acta Crystallogr. C65 (2009) 11–13.
[11] A. Magrasó, R. Haugsrud, T. Norby, J. Am. Ceram. Soc. 93 (9) (2010) 2650–2655.
[12] D.M. Kepaptsoglou, et al., Unpublished work.
[13] M.F. Sunding, D.M. Kepaptsoglou, S. Diplas, T. Norby, A.E. Gunnæs, Surf. Interface Anal. 42 (2010) 568–571.
[14] J.R. Tolchard, H.L. Lein, T. Grande, J. Eur. Ceram. Soc. 29 (2009) 2823–2830.
[15] L. Bail, H. Duroy, J.L. Fourquet, Mater. Res. Bull. 23 (3) (1988) 447–452.
[16] E.V. Tkachenko, F.A. Abbattista, A. Burdese, Izv. Akad. Nauk SSSR, Neorg. Mater. 5 (11) (1969) 1963–1968;
E.V. Tkachenko, F.A. Abbattista, A. Burdese, Inorg. Mater. (Engl. Transl.) 5 (11) (1969) 1671–1674.
[17] K. Kitayama, J. Solid State Chem. 83 (1) (1989) 37–44.
[18] O. Khamman, R. Yimnirun, S. Ananta, Mater. Lett. 61 (2007) 2565–2570.
[19] T.S. Stokkan, Personal communication.
[20] R.C. Pullar, J. Am. Ceram. Soc. 92 (3) (2009) 563–577.
[21] A. Orera, F. Garcia-Alvarado, J.T.S. Irvine, Chem. Mater. 19 (9) (2007) 2310–2315.
[22] F. Garcia-Alvarado, A. Orera, J. Canales-Vazquez, J.T.S. Irvine, Chem. Mater. 18 (16) (2006) 3827–3834.
[23] M. Lopez-Blanco, U. Amador, F. Garcia-Alvarado, J. Solid State Chem. 182 (2009) 1944–1949.
[24] S.A. Shtin, A.L. Podkorytov, Yu.S. Khlupin, S.R. Kudakaeva, E.V. Sokolova, K.A. Khuramshina, Inorg. Mater. 46 (11) (2010) 1274–1279.
[25] M. Huse, Transport and hydration in acceptor doped proton conducting oxides-effect of proton-acceptor associations, Ph.D. Thesis, University of Oslo.
[26] H.L. Lein, T. Tezuka, T. Grande, M.-A. Einarsrud, Solid State Ionics 179 (21–26) (2008) 1146–1150.
[27] M.-L. Fontaine, Y. Larring, R. Haugsrud, T. Norby, K. Wiik, R. Bredesen, J. Power Sources 188 (1) (2009) 106–113.
[28] A. Magrasó, H. Xuriguera, M. Varela, M.F. Sunding, R. Strandbakke, R. Haugsrud, T. Norby, J. Am. Ceram. Soc. 93 (7) (2010) 1874–1878.